Soft Matter

Friction between Ring Polymer Brushes

Journal:	*Soft Matter*
Manuscript ID:	SM-ART-12-2014-002818.R3
Article Type:	Paper
Date Submitted by the Author:	24-Feb-2015
Complete List of Authors:	Erbas, Aykut; Northwestern University, Paturej, Jaroslaw; Leibniz-Institut of Polymer Research,

Friction between Ring Polymer Brushes

Aykut Erbas
Northwestern University,
Department of Materials Science and Engineering
Evanston, IL 60208, USA

Jarosław Paturej
Leibniz-Institut of Polymer Research, 01069 Dresden, Germany and
Institute of Physics, University of Szczecin, Wielkopolska 15, 70451 Szczecin, Poland

(Dated: February 24, 2015)

Friction between ring polymer brush bilayers at melt densities sliding past each other are studied using extensive coarse-grained molecular dynamics simulations and scaling arguments, and the results are compared to the friction between bilayers of linear polymer brushes. We show that for a velocity range spanning over three decades, the frictional forces measured for ring polymer brushes are half of the corresponding friction in the case of linear brushes. In the linear-force regime, the weak inter-digitation between ring brush layers as compared to linear brushes leads also to a lower number of binary collisions between the monomers from opposing brushes. At high velocities, where the thickness of the inter-digitation between bilayers is on the order of monomer size regardless of brush topology, stretched segments of ring polymers adopt the double-stranded conformation. As a result, monomers of the double-stranded segments collide on average less with the monomers of the opposing ring brush even though a similar number of monomers occupies the inter-digitation layer for ring and linear brush bilayers. The numerical data obtained from our simulations is consistent with the proposed scaling analysis. Conformation-dependent friction reduction observed in ring brushes can have important consequences in non-equilibrium bulk systems.

INTRODUCTION

If polymer chains are grafted by one of their ends to a planar or curved surface, above a certain critical grafting density $\sigma_g^* \approx 1/R_0^2$ [1], where R_0 is the characteristic equilibrium chain size, the chains are stretched away from the surface due to steric repulsion from surrounding chains and form polymer brush. A polymer brush is a soft polymeric material that can deform under various external forces. The external force can be due to a fluid flowing over the brush, a flow due to the relative motion of a second brush, or alternatively, an external electrical field (if polymers are charged). Once the external stimulus is completely removed, as the chains constituting brush relax, deformation of brush is reversed similar to the elastic deformation observed for solids. However, the tribological behaviour of polymeric systems resembles more that of a fluid rather than a solid [2]. For instance, if two inter-digitated polymer brushes are slid past each other, frictional forces due to the relative motion of brushes vanish linearly as the relative velocity of the brushes is decreased towards zero. In other words, the friction is viscous and no static friction occurs, unlike the solid-state friction, where finite forces are needed to initiate motion [3].

Polymer brushes has attracted increasing attention due to their applications in nanotechnology and material sciences as bio-sensors, bio-fueling, stimuli-responsive surfaces [4–8], or for the stabilisation of colloidal solutions [9, 10]. The most fascinating application of brush-like structures is facilitated by nature in maintaining the lubrication in tissues [11–14]. For instance, in mammalian joints, where very low lubrication should be retained under pressures as high as 5 MPa, brush-like structures in combination with the synovial fluid provide lubrication in between the articular joints [14–16]. The surfaces separating the articular cartilage and the synovial fluid are thought to be covered by high molecular weight molecules such as lubricin [14, 17]. In turn, these long and charged glycoproteins may function as water-based bio-lubricants. The relationship between morphology of these long and charged macromolecules on the cartilage surfaces and their function in lubrication is still under investigation [11, 14, 16–20]. Amphiphilic lubricin chains can adsorb on both hydrophilic and hydrophobic surfaces [16, 21], but their conformations in the adsorbed state strongly depend on the type of surface. These molecules can bind onto hydrophilic surfaces via their charged domains located in the central part of a molecule and form structures resembling a brush composed of linear chains. Alternatively, they can also bind onto hydrophobic surfaces with their terminal groups to form loop brush-like structures [16, 21, 22]. Hence, based on the experimental observations and variations in the molecular conformations *in vitro*, one may conclude that in reality the whole cartilage surface resembles a polymer brush composed of linear and loop-like chains. Although molecules mentioned so far are highly charged, and long-range interactions might be a dominant factor in reduction of frictional forces, conformation of chains – whether they are linear or looped – can influence inter-digitation of molecules as well as their relaxation times, and hence,

friction and lubrication in tissues.

Inter-digitation effects due to ring topology have also been reported in the context of genetic material: in a computational study, unconcatenated chains of ring polymers showed a weak trend towards inter-mixing with each other compared to mixing behaviour of linear chains in confined environments [23]. We should also underline that static properties of ring polymers in bulk and at melt densities exhibit different behaviour with respect to their linear counterparts [24, 25]. The behaviour of ring polymers cannot be described by single fractal dimension unlike linear chains in melts: while size of a linear chain at melt state scales as $R_{0L} \sim N^{1/2}$, a ring polymer in the melt of rings is much more compact and the characteristic size scales as $R_{0R} \sim N^{1/2}$ for short chains and $R_{0R} \sim N^{1/3}$ for sufficiently large polymerization degree N. In between these two limits, an intermediate regime $R_{0R} \sim N^{2/5}$ arises [24, 25]. Moreover, even in the regimes where the size of ring chain is non-Gaussian, interestingly higher moments of the end-to-end distance exhibit a Gaussian-like behaviour [24].

In the last two decades the sheared linear polymer brush bilayers have been extensively explored using both theory [26–30] and simulations [26, 31–44]. Existing studies on linear polymer brushes have shown that frictional forces acting between brushes exhibit a cross-over from a linear to a non-linear regime upon increasing shear velocity. The onset of non-linear friction typically appears at shear rates where grafted chains begin to stretch. Ideally, one would expect a similar behaviour in the case of ring-polymer brushes. However, how the topology and peculiar scaling of ring chains alter the friction is an open question. To the best of our knowledge there are very few computational investigations of ring polymer brushes out of equilibrium [45, 46]. In a previous work [46], tribology of loop brushes near the overlap concentrations were studied, but the observed difference in frictional forces was negligible. However, at melt densities where the correlation length – distance between two chains – is on order of monomer size, the situation can be different as the number of collision between brush monomers can significantly increase in a denser system.

Characterizing the systematic reduction in brush friction due to the topology of the constituting chains can improve our understanding of how nature handles friction and help to design and improve new advanced biomimetic lubricants. Thus, spurred by the abundance of brush-like structures in biological systems and the interesting nature of ring polymers themselves in this paper we aim to study non-equilibrium behaviour of ring-polymer brushes at melt densities. In our extensive coarse-grained MD simulations, we used neutral (uncharged) polymer brushes. Given the fact that the system we would like to mimic is under high pressure (e.g., in joints), and ionic condensation (short Debye length in physiological conditions) can effectively neutralize chains, we believe that this approximation is reasonable for the sake of minimizing computational cost [32] since long-range electrostatic interactions are known to be computationally expensive, particularly for dense systems. Through a detailed analysis of simulation trajectories and by employing scaling arguments, we demonstrate that the topology of chain in a polymer brush is an important factor in the reduction of frictional forces.

In our simulations, we found that for untangled brushes friction forces between two brushes made of linear chains are always roughly a factor of two higher than those for ring chains. Although this difference is small, it persists for various grafting densities and chain sizes. The difference in frictional forces of ring and linear brushes can be elucidated by the size of the overlap zone, which defines the amount of inter-digitation between two brushes. It turns out that the low tendency of ring chains to overlap with the opposing ring-brush leads to lower friction forces whereas linear chains can diffuse through the opposing brush more easily. Hence, brushes made of linear chains exhibit higher frictional forces. At very high velocities, segments of a ring brush adopt a double-stranded conformation. In turn, double-strands are less efficient in momentum transfer between the opposing brushes. The difference in friction forces between both systems is confirmed by scaling analysis.

The paper is organized as follows: First we briefly describe the simulation methodology. Next, the results obtained from non-equilibrium coarse-grained brush simulations will be discussed. We relate the difference in friction forces to the intrinsic properties of ring and linear (grafted) chains. The scaling arguments for brush systems are discussed to infer the difference in forces along with the simulations data. We conclude the paper with the summary of our findings and future prospects.

SIMULATION DETAILS

Simulations of polymer brush bilayers were performed using coarse-grained Kremer-Grest (KG) bead-spring model [47]. Each individual chain of a polymer brush was composed of N (or $2N$) monomers (beads) connected by bonds. The non-bonded interactions between monomers separated by distance r were modeled by the truncated and shifted Lennard-Jones (LJ) potential

$$V^{\mathrm{LJ}}(r) = \begin{cases} 4\epsilon\left[(\sigma/r)^{12} - (\sigma/r)^{6} + c\right] & r \le r_c \\ 0 & r > r_c \end{cases} \quad (1)$$

where the interaction strength ϵ is measured in units of thermal energy k_BT, σ is chosen as the unit of length, r_c is the cutoff and c is the shift introduced to avoid discontinuity of potential at r_c. The simulations were carried out with the following parameters $\epsilon = k_BT$, $c = 1/4$ and $r_c = 2^{1/6}\,\sigma$. The choice of LJ potential cutoff r_c results

in purely repulsive interactions between monomers which in combination with a monomer density of $\rho_m \approx 0.6\,\sigma^{-3}$ provides correct melt statistics [26, 32, 48]. The bonded interactions in a molecule were described by the Kremer-Grest potential, $V^{\rm KG}(r) = V^{\rm FENE}(r) + V^{\rm LJ}(r)$ with the "finitely extensible nonlinear elastic" (FENE) potential:

$$V^{\rm FENE}(r) = \begin{cases} -\frac{1}{2}kr_0^2 \ln\left[1 - \left(\frac{r}{r_0}\right)^2\right] & r \le r_0 \\ \infty & r > r_0 \end{cases} \quad (2)$$

where $k = 30\,\epsilon/\sigma^2$ is bond stiffness and $r_0 = 1.5\,\sigma$ is maximum bond length [47].

Polymer brushes composed of chains with either linear or ring-like topology were studied. We performed simulations with linear-polymer brushes composed of $N = 60$, 100 monomers, and ring-polymer brushes of $N = 120$, 200 monomers per grafted chain. Chains were grafted on a square-lattice surface with dimensions $42\,\sigma \times 36\,\sigma$. The ring chains were grafted by one of their monomers on the surface. No equation of motion was solved for surface monomers (surface monomers were immobile during simulations). The surface and the brush monomers interact via interaction given in Eq. (1). The grafting densities of linear chains are $\sigma_g^L = 0.11\,\sigma^{-2}, 0.25\,\sigma^{-2}$, which respectively corresponds to inter-anchored monomer distances of $3\,\sigma\,, 2\sigma$ at the surface. In the case of ring brushes, to obtain an equal monomeric density ($\rho_m \approx 0.6\ \sigma^{-3}$) as compared to the linear brushes, the grafting densities were taken as $\sigma_g^R = 0.5\sigma_g^L$ at the same inter-plate distance D. Note that D and $\sigma_g^{L,R}$ are connected via $\rho_m \approx N\sigma_g^{L,R}/D$. In order to construct brush bilayer systems, first two non-interacting single brushes were generated as mirror images of one another. While one of the brushes is fixed at $z = 0$, the other brush is brought into contact slowly at the desired inter-plate distance $z = D$ to obtain the same monomer density for each $\sigma_g^{L,R}$ and N. Finally, the systems were run at velocity $v = 0$ (no shear) for at least 10^7 MD steps to allow chains to relax.

The molecular dynamics simulations were performed by solving the Langevin equation of motion, which describes the Brownian motion of a set of interacting monomers, as

$$m\ddot{\mathbf{r}}_i = \mathbf{F}_i^{\rm LJ} + \mathbf{F}_i^{\rm FENE} - \Gamma\dot{\mathbf{r}}_i + \mathbf{F}_i^{\rm R}, \quad i = 1, \ldots, N, \quad (3)$$

where $\mathbf{r}_i = [x_i, y_i, z_i]$ is the position of i–th monomer. $\mathbf{F}_i^{\rm LJ}$ and $\mathbf{F}_i^{\rm FENE}$ in Eq. (3) are respectively LJ and FENE forces exerted on the i–th monomer and given by derivatives of Eqs. (2) and (1) with respect to $\mathbf{r}_i$. The effect of the implicit solvent in Eq. (3) is split into a slowly evolving viscous force $-\Gamma\dot{\mathbf{r}}_i$ and a rapidly fluctuating stochastic force $\mathbf{F}_i^{\rm R}$. This random force $\mathbf{F}_i^{\rm R}$ is related to the friction coefficient Γ by the fluctuation-dissipation theorem $\langle \mathbf{F}_i^{\rm R}(t)\mathbf{F}_j^{\rm R}(t')\rangle = k_BT\Gamma\delta_{ij}\delta(t-t')$. The friction coefficient used in simulations was $\Gamma = 0.5\,m\tau^{-1}$, where

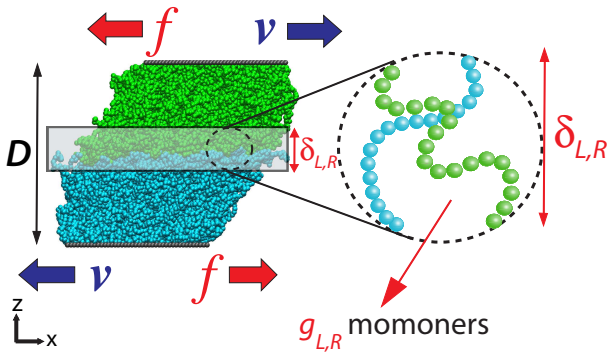

FIG. 1: Scheme of brush bilayer shear simulation. The force f acts in the direction opposite to velocity v. Chains at the top and bottom brush are rendered in different colors. The overlap zone (OZ) with thickness $\delta_{L,R}$ is indicated by a milky-white region. The dashed circle shows the segments of chains with $g_{L,R}$ monomers inside the penetration zone. Here $N = 60$, $\sigma_g^L = 0.25\ \sigma^{-2}$ and $D = 50\ \sigma$. Images are obtained via VMD.

$m = 1$ is the monomer mass and time was measured in units of $\tau = \sqrt{m\sigma^2/\epsilon}$. The integration step was taken to be $\Delta\tau = 0.002\,\tau$. The velocity Verlet scheme was used for numerical integration of equations of motion Eq. (3). All simulations were performed in the N_mVT-ensemble, i.e. at constant volume V, total particle number N_m and temperature T. The system temperature was set to the value $T = 1.68\ \epsilon/k_B$ with $k_B = 1$ [48, 49]. Periodic boundary conditions were introduced in the lateral directions, i.e. in $\hat{x}$ and $\hat{y}$ whereas in the $\hat{z}$-direction fixed boundary conditions were imposed. Simulations were carried out using molecular package LAMMPS [50]. Simulation snapshots were rendered using Visual Molecular Dynamics (VMD) [51].

The non-equilibrium shear simulations were performed as shown in Fig. 1. Both plates grafted by polymers were moved laterally in the opposite ($\pm\hat{x}$-directions) at prescribed velocities in a range of $v \approx 10^{-3}\,\sigma/\tau$ and $v \approx 1\,\sigma/\tau$. The inter-plane distance D was kept constant during shearing. For each plate velocity, all system were run for 10^7 MD steps until the steady state in friction force was reached, i.e. error bars in time-averaged quantities were independent of simulation time. Error bars were calculated via block-averaging. For the purpose of data analysis, additional simulations were run for 10^6 up to 10^8 MD simulation steps depending on the velocity and in order to obtain proper plate displacements. As a rule each plate was displaced by at least 5 times in the corresponding $\pm\hat{x}$-directions. To avoid any bias on friction forces or vertical chain diffusion while the system was sheared, the thermostat was applied only in the $\hat{y}$-direction [31, 48].

In this paper, we report frictional forces which are

the forces acting on the plates due to relative motion of brushes. If there is no contact between brush bilayers, the friction force is zero. To keep the plates at the prescribed velocity, at each timestep the external force was subtracted from the friction force to obtain a zero total force on each plate. Averaged brush properties were calculated from monomer trajectories. Unless otherwise noted, all results presented in this paper were averaged over time.

RESULTS AND DISCUSSION

In the course of simulations, two compressed polymer brushes were moved in the opposite ($\pm\hat{x}$) directions by driving both planes grafted by chains at prescribed velocities v as shown in Fig 1. Each plane experiences a friction force in the opposite direction to its motion due to relative motion of brushes. In Fig. 2, the friction force for linear brushes f_L (filled symbols) and for ring brushes f_R (open symbols) are shown as a function of velocity v, for various brush systems with different polymerization degrees N and chain topologies. The overall velocity dependence of friction forces is consistent with previously reported results [26, 32, 33, 52]: The frictional force increases linearly up to a threshold velocity, which occurs at different velocities for different brush bilayers. Above a threshold velocity, a sublinear increase occurs for all brush systems considered here. The velocity dependence of the friction force within the non-linear regime for both linear and ring brushes was found to be in perfect agreement with the scaling $f_L \sim v^{0.55\pm0.03}$ reported by several groups [26, 32, 33]. We observe this linear-to-sublinear transition in most of our systems except the case with inter-plate distance $D = 35\,\sigma$, where only the onset of the non-linear regime can be seen in Fig. 2d. As we will discuss in more details in the following sections, this is due to the fact that the threshold velocity separating the linear and non-linear force regimes depends on segment size inside the overlap volume, where two opposing brushes can co-exist. Hence, as the size of the average segments increases inside the overlap volume, much slower velocities are required to observe the linear-force regime. The comparison of friction forces acting on linear and ring brushes, which is the main motivation of this work, shows that friction forces for linear brushes are always higher than those acting on ring brushes, i.e. $f_L > f_R$. The numerical value of the ratio between these two forces is $f_L/f_R \approx 2$ as can be seen in the insets of Fig. 2. The ratio holds for a broad range of shearing velocities ($v \approx 10^{-3}$-$10^{0}\,\sigma/\tau$).

Average normal forces acting on the plates in the $\hat{z}$-direction were also measured. We observe that normal pressure exhibit a weak dependence on velocity, i.e. a three order of magnitude increase in velocity leads to a roughly 10% increase in the normal forces for both linear and ring brushes (data not shown). At high velocities, a slight decrease in all measured pressures is observed. Similar to the frictional forces, the normal pressures measured for linear brushes are factor of two higher than ring brushes, $p_z^L/p_z^R \approx 2$. However, if total normal forces are rescaled by the number of grafted chains for each system, normal forces per chain are of almost equivalent in both systems.

TABLE I: The equilibrium values of the thickness of the overlap zone (OZ) $\delta_{0L,0R}$ (calculated via Eq. 4) and number of monomers $g_{0L,0R}$ per segment of a chain located inside the OZ for linear and ring brush bilayers with various inter-plate distances D and grafting densities $\sigma_g^R = 0.5\sigma_g^L$. The number of monomers per segment is denoted by N.

	Linear brush				Ring brush			
$D[\sigma]$	$\sigma_g^L[\sigma^{-2}]$	N	$\delta_{0L}[\sigma]$	g_{0L}	$\sigma_g^R[\sigma^{-2}]$	N	$\delta_{0R}[\sigma]$	g_{0R}
50	0.25	60	2.97	9	0.125	120	2.47	15
22	0.11	60	4.88	22	0.055	120	3.81	37
80	0.25	100	3.82	12	0.125	200	2.91	21
35	0.11	100	6.05	33	0.055	200	4.62	53

In what follows, we discuss the observed difference in the frictional forces acting on linear and ring brushes. We consider linear and non-linear force regimes separately and demonstrate that the ratio $f_L/f_R \approx 2$ is related to the topology of chains and of their velocity-dependent conformations.

Linear regime

In this subsection we consider the regime where frictional forces increase linearly with the driving velocity v (Fig. 2). If two dense polymer brushes are brought into contact at the inter-plate distance $D > R_0$, as shown in Fig. 1, where R_0 is equilibrium size of a free chain in bulk, chain segments near the free ends can interpenetrate through the opposing brush. Hence, an overlap zone (OZ), where monomers of opposing brushes can mutually interact, can be defined as illustrated in Fig. 1 by a rectangular region.

From simulation trajectories, the thickness of the OZ can be obtained using the cross product of monomer density profiles of top $\rho_{\rm top}(z)$ and bottom $\rho_{\rm bott}(z)$ brushes for each velocity. The cross product is non-zero only if monomers from both parts of brush coexist at the same z coordinate. The width of the OZ can be calculated from

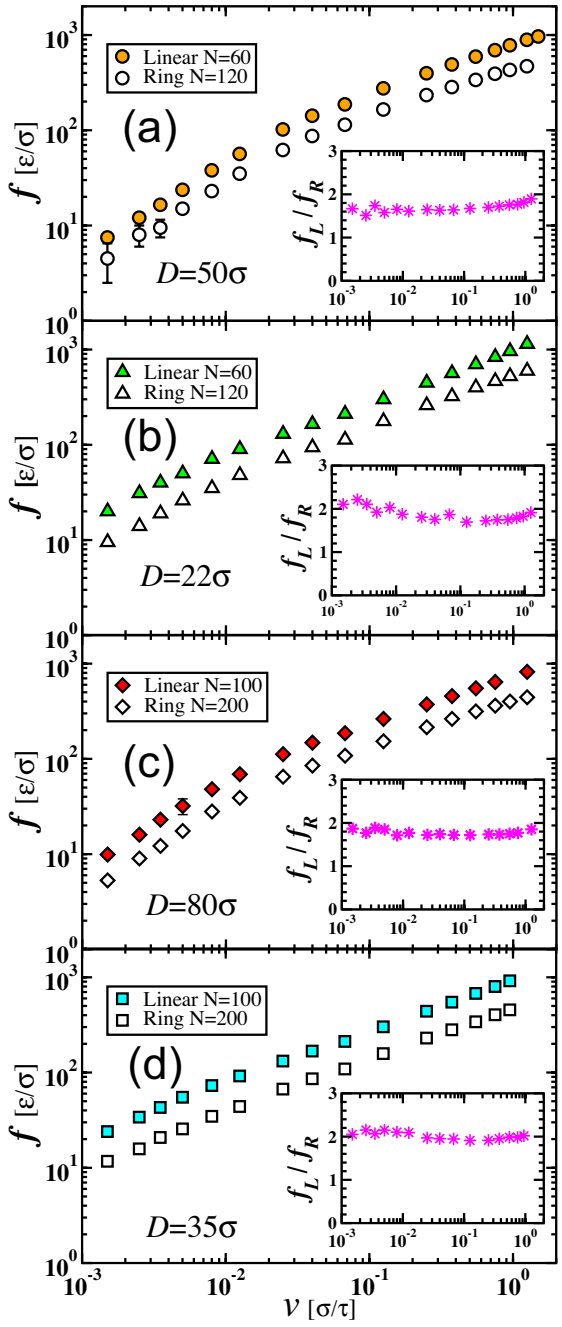

FIG. 2: Total friction forces f as a function of plate velocity v for linear and ring brushes. The grafting densities are for a) $\sigma_g^L = 0.25\sigma^{-2}$ b) $\sigma_g^L = 0.11\sigma^{-2}$ c) $\sigma_g^L = 0.25\sigma^{-2}$ d) $\sigma_g^L = 0.11\sigma^{-2}$ with $\sigma_g^R = 0.5\sigma_g^L$ for all plots.

the cross-product-weighted averages as

$$\delta^2(v) \equiv \langle z^2 \rangle - \langle z \rangle^2 \qquad (4)$$
$$\equiv 4 \left[\int_{-D/2}^{D/2} z^2 \omega(z) dz - \left(\int_{-D/2}^{D/2} z \omega(z) dz \right)^2 \right],$$

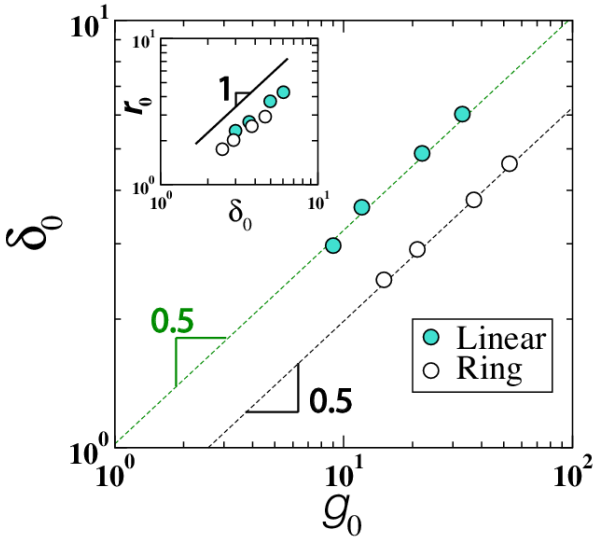

FIG. 3: The equilibrium values of the width of the overlap zone (OZ) versus number of monomers g_0 per segment of a chain located inside the OZ for linear (full symbols) and ring (empty symbols) brushes. Dashed lines represent fitted power laws: $\delta_0 \approx 1.0 g_0^{1/2}$ (for linear chains) and $\approx 0.625 g_0^{1/2}$ (for rings). The inset shows fluctuation of the end-to-end size of segments $r_0 \equiv \langle r_0^2 \rangle^{1/2}$ inside the OZ as a function of δ_0. Solid line shows the scaling $r_0 \sim \delta_0$. See also Table I.

where the normalized cross product was defined as $\omega(z) \equiv \rho_{\rm top}(z)\rho_{\rm bott}(z)$ such that $\int_{-D/2}^{D/2} \omega(z) dz = 1$. Eq. 4 is valid for any brush for which $D > R_0$. In the case of $D \approx R_0$ the thickness of the OZ is $D \approx \delta$. Note that for symmetric bilayers the first moment $\langle z \rangle$ is zero. In Fig. 4 monomeric density profiles $\rho_{\rm top}(z)$ and $\rho_{\rm bott}(z)$ and their products $\rho_{\rm top}(z)\rho_{\rm bott}(z)$ are shown for both linear (solid lines) and ring (dashed lines) brush bilayers at $v = 0$. While outside of the OZ the monomeric density profiles are uniform along the simulation box, inside the OZ chains from the top brush can only penetrate a finite distance δ from the bottom brush. The distance δ is defined by Eq. 4.

The equilibrium value of the OZ thickness can be obtained from simulations without shear, i.e. $\delta(v = 0) \equiv \delta_0$. Note that in this paper we use subscript "zero" to indicate equilibrium, i.e. at a plate velocity $v = 0$, or linear-response values of corresponding parameters whereas subscripts L and R refer respectively to linear and ring brushes. The equilibrium values of the widths of the OZ for linear and ring brushes $\delta_{0L,0R}$ are shown in Fig. 3 as a function of the number of monomers $g_{0L,0R}$ per participating chain for linear and ring brushes (see also Table I which lists the numerical values of both quantities). As a rule a chain is considered as "participating", i.e. being present inside the OZ, if z coordinate of the N-th monomer of the corresponding chain satisfies

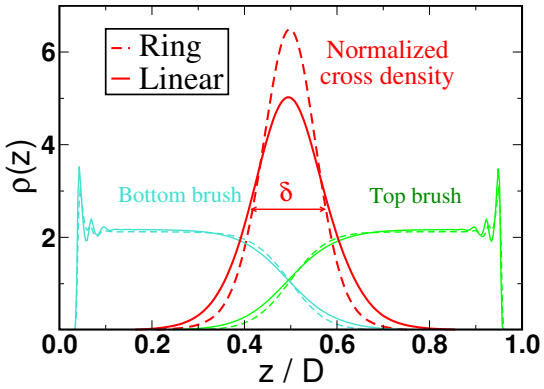

FIG. 4: The equilibrium monomer density profiles $\rho(z)$ for linear (solid lines) and ring (dashed lines) brush bilayers plotted as a function of the rescaled vertical distance between plates z/D. The red curves display cross products of densities of top and bottom layers; the width of these distribution given by Eq. 4 defines the overlap zone of brush bilayer. Here for linear brushes $N = 100$ and $\sigma_g^L = 0.11\ \sigma^{-2}$ whereas for ring brushes $N = 200$ and $\sigma_g^R = 2\sigma_g^L$. The inter-plate distance for both cases is $D = 35\ \sigma$.

the following condition: $D/2 - \delta_{L,R} < z < D/2 + \delta_{L,R}$. As we perform our simulations nearly at melt density ($\rho_m \approx 0.6\,\sigma^{-3}$), the random-walk statistics allows us to express the end-to-end distance of a segment with $g_{0L,0R}$ monomers as $r_{0L,0R} \equiv \langle r^2_{0L,0R}\rangle^{1/2} \sim g^{1/2}_{0L,0R}$ for short enough segments. If the size of the segment determines the width of the OZ, the relation $r_{0L,0R} \approx \delta_{0L,0R}$ should hold. Indeed, this is what we observe in Fig. 3 and in its inset for both linear and ring brushes: $r_{0L,0R} \approx \delta_{0L,0R} \sim g^{1/2}_{0L,0R}$. Interestingly, we found that at the same inter-plate distance D, a chain in a ring brush occupies the overlap volume filled with more monomers than a chain in a linear brush ($g_{0R} > g_{0L}$). This finding demonstrates that the segments of ring brushes are more compact inside the OZ as compared to segments of linear brushes. This is also supported by Fig. 3 since the pre-factor of the power-law fit is 1.6 times larger for linear brushes. The compactness of segments in ring brushes yields to a narrower OZ. As a remark, for very long segments in ring brushes ($g_R \gg 1$) the width of the OZ should in the asymptotic limit converge to $\langle r^2_{0R}\rangle^{1/2} \approx \delta_{0R} \sim g^{1/3}_{0R}$. In that case: $\delta_{0L}/\delta_{0R} \sim g^{1/2}_{0L}/g^{1/3}_{0R}$.

Since two opposing brushes can only interact inside the OZ, the observed frictional forces should be related to the width of OZ. The grafted chains are not static as they constantly diffuse in and out of the overlap volume which is given by $A \times \delta_{L,R}$ where A is the area of a grafting plate due to thermal fluctuations. When two plates are moved at nonzero velocity $v > 0$, any chain segment that enters the OZ feels a flow induced by the relative motion of monomers moving in the opposite direction. The force acting on each monomer inside the overlap volume can be most generally expressed via Stokes drag $f_m \approx \zeta v$, where ζ is the monomeric friction coefficient. The total friction force acting on $\rho_m A\delta$ monomers inside the overlap volume can be expressed for both linear and ring brushes as follows

$$f_{L,R} \approx \zeta_0 v \rho_m \delta_{L,R} A \Omega_{L,R}. \tag{5}$$

In Eq. (5), we introduced $\Omega_{L,R}$ which quantifies the number of binary collisions between the monomers of two opposing brushes and depends on the topology of grafted chains. As we will see shortly, although there are $\rho_m \delta A$ monomers inside the overlap volume, only a fraction of them participate in momentum exchange between opposing brushes. Hence, $\Omega_{L,R}$ is an important quantity to distinguish the friction among different brush systems. In addition, the equilibrium value of the monomeric friction coefficient ζ_0 is expected to be equal for monomers of both linear and ring brushes. Indeed, calculated force per monomer inside the overlap volume at a specific velocity does not show any difference for ring and linear brushes (data not shown). This is due to the fact that on the time scales comparable with time between inter-bead collisions monomer cannot know whether it belongs to a linear or ring chain.

Based on the linear-response theory, which states that any fluctuation takes its equilibrium value if the perturbation is small, we replace the quantities appearing in Eq. (5) with their equilibrium values as $v \to 0$, i.e., $\delta_L \approx \delta_{0L}$ and $\delta_R \approx \delta_{0R}$ and similarly $\Omega_L \approx \Omega_{0L}$ and $\Omega_R \approx \Omega_{0R}$. Thus, the frictional force ratio in the linear-force regime reads

$$\frac{f_L}{f_R} \approx \frac{\delta_{0L}\Omega_{0L}}{\delta_{0R}\Omega_{0R}}. \tag{6}$$

The validity of Eq. (6) can be verified from the simulation data by calculating the equilibrium values of $\delta_{L,R}$ and $\Omega_{L,R}$ for both linear or ring brushes. From now on, to keep the manuscript more compact we will only show data from four of our eight brush systems. All comparisons and discussions are valid for the systems which are not shown here as well. We show results of non-equilibrium simulation for the thickness of OZ $\delta_{L,R}$ as a function of plate velocity v for various linear and ring brushes in Fig. 5. Each frame of Fig. 5 compares the OZ width of ring brushes (open symbols) to those obtained for linear brushes (filled symbols) at the same inter-plate distance D. Independently of the chain topology the width of the OZs exhibit a plateau for all brush systems as $v \to 0$. The plateau values of the OZs, which are $\delta_L \approx \delta_{0L}$ and $\delta_R \approx \delta_{0R}$, persist up to the plate velocities, around which the linear-force regime observed in Fig. 2 ends. Indeed, as we proposed in Eq. 6, the widths of OZs $\delta_{L,R}$ are equal to their equilibrium values. This

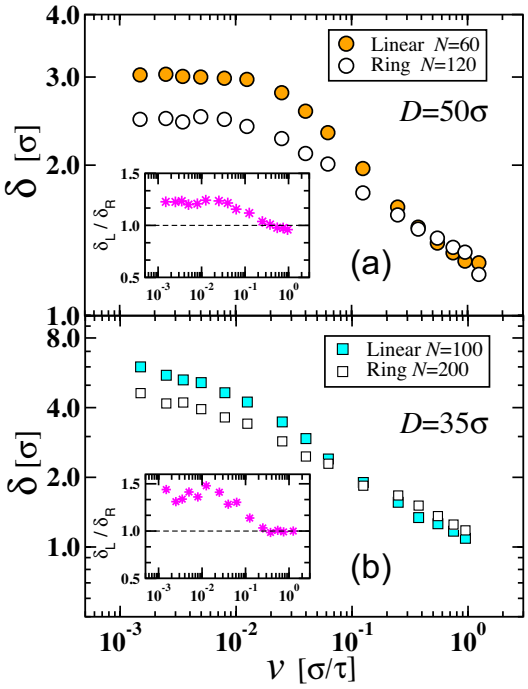

FIG. 5: The thickness δ of the overlap zone for linear and ring brushes plotted as a function of plate velocity v. The values of δ were calculated using Eq. (4). The insets show the ratios. The grafting densities are a) $\sigma_g^L = 0.25\sigma^{-2}$ and b) $\sigma_g^L = 0.11\sigma^{-2}$ with $\sigma_g^R = 0.5\sigma_g^L$ for all plots.

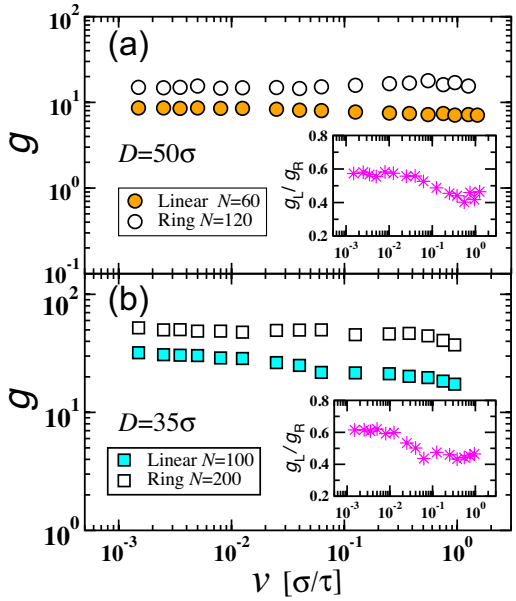

FIG. 6: The number of monomers g inside the overlap zone per participating chain for ring and linear brush bilayers as a function of the plate velocity v. Insets show the ratios. The grafting densities are a) $\sigma_g^L = 0.25\sigma^{-2}$ and b) $\sigma_g^L = 0.11\sigma^{-2}$ with $\sigma_g^R = 0.5\sigma_g^L$ for all plots.

is due to the fact that within the linear-force regime, for which frictional forces change linearly with velocity, values of $\delta_{0L,0R}$ are given by the fluctuations in size of a chain segments in the $\hat{z}$-direction inside the OZ (Fig. 3). The size of a segment with $g_{L,R}$ monomers defines the width of the OZ as also illustrated in Fig. 1.

The number of monomers per segment $g_{L,R}$ inside the OZ for linear and ring brushes was analyzed and is shown in Fig. 6 as a function of the plate velocity v using the same color code as in Figs. 2 and 5. In the entire velocity range considered here the following ratio holds $g_R \approx 2g_L$ for the same value of D. At slow velocities ($v \to 0$) the ratio of monomers per segment g_{0L}/g_{0R} is ≈ 0.6. The ratio drops to $g_L/g_R \approx 0.4$ at higher velocities ($v > 10^{-1}\,\sigma/\tau$).

Similar trajectory analysis was also conducted to determine the number of binary collisions $\Omega_{L,R}$ inside the overlap volume. To count collisions, distances between the monomers from opposing brushes were calculated. If the distance is equal or smaller than the cutoff distance of LJ potential r_c defined in Eq. (1), this specific pair is counted as a colliding pair. To obtain $\Omega_{L,R}$ and compare the number of collisions for ring and linear chains, the total number of collisions is rescaled by the corresponding value of $\rho_m A\delta_{L,R}$. In Fig. 7, we show the binary-collision fractions $\Omega_{L,R}$, as well as their ratios in the insets. Interestingly, for linear brushes there are more collisions as compared to ring brushes, i.e. $\Omega_L > \Omega_R$ for the entire velocity range although $g_R \approx 2g_L$. An average ratio of $g_L/g_R \approx 0.5$ indicate that a single chain in ring brushes can occupy the overlap volume with more monomers than a chain in linear brushes ($g_R > g_L$). The compactness of the segments in ring brushes yield to a narrower OZ (Fig. 3). The compactness also suppresses inter-brush collisions between the monomers of opposing brushes. Since some monomers of the segments in ring brushes are shielded from collisions, we found $\Omega_L > \Omega_R$ and consequently $f_L > f_R \approx 2$.

Values of Ω_L and Ω_R as $v \to 0$ in Fig. 7 are close to values obtained in equilibrium simulations, i.e., $\Omega_L \approx \Omega_{L0}$ and $\Omega_R \approx \Omega_{0R}$. At the same plate separation D, the ratios of plateau values are $\delta_{0L}/\delta_{0R} \approx 1.3 \pm 0.05$ from Fig. 5 and $\Omega_{0L}/\Omega_{0R} \approx 1.7 \pm 0.1$ from Fig. 7. Plugging the later expression into Eq. 6 gives the ratio of friction force for the linear-force regime $f_L/f_R \approx 2.3$, which is consistent with the ratios of forces obtained in the insets of Fig. 2).

As the frictional forces increase linearly (see Fig. 2) in principle none of terms in Eq. (5) should be velocity dependent. Indeed, this is what one would expect at the linear-response level: at slow enough velocities ($< 10^{-1}\,\sigma/\tau$) the conformation of chain segments within the OZ are not affected by the velocity. As a result, the

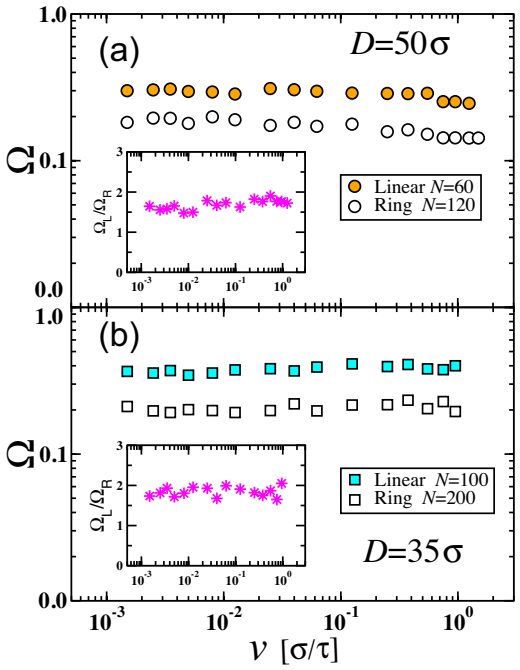

FIG. 7: The binary-collision factor Ω inside the overlap zone between two brushes as a function of the plate velocity v. See the text for details. Insets show the ratio of linear-brush and ring-brush data. The grafting densities are a) $\sigma_g^L = 0.25\sigma^{-2}$ and b) $\sigma_g^L = 0.11\sigma^{-2}$ with $\sigma_g^R = 0.5\sigma_g^L$ for all plots.

ratios of forces for linear and ring brushes are constant and given by Eq. (6).

Our analyzes confirm that in ring brush bilayers, the amount of inter-digitation of chains is weaker compared to that in linear brush bilayers at slow driving velocities, where the friction increases linearly with velocity.

Non-linear regime

In this subsection we will focus on the regime where frictional forces demonstrate sublinear plate velocity v dependence. As can be seen in Fig. 2 nonlinear regime is observed for both linear and ring bilayers. Another indication of the non-linear regime is the shrinkage of the overlap volume with increasing velocity v (shear thinning) as shown in Fig. 5. Onset of the non-linear regime occurs at a threshold velocity $v = v^*$. Indeed, v^* has different values for different chain sizes as can be noticed in Figs. 2 and 5. Before we further continue our discussion on the non-linear regime, we will briefly discuss two scaling predictions for the threshold velocity, and refer them as v_I^* and v_{II}^*.

We will temporarily drop the indexes for ring and linear brushes for simplicity and refer $g_0 \equiv g_{0L} \equiv g_{0R}$ and $\delta_0 \equiv \delta_{0L} \equiv \delta_{0R}$, etc. If a segment with g_0 monomers enters the OZ, the force acting on this segment in the linear regime can be expressed as $f_{ch} \approx \zeta_0 g_0 v$. As we have discussed in the previous section, below the threshold velocity the chains are still Gaussian. Hence, as expected from a Gaussian chain, segment chain sizes in $\hat{x}$, $\hat{y}$ and $\hat{z}$-directions are not coupled, i.e. fluctuations in segment size in all direction are independent of each other. However, as the velocity is increased, the frictional force per segment inside the OZ reaches a threshold force $f_{ch}^* \approx k_BT/b \approx \zeta_0 g_0 v_I^*$ at $v = v_I^*$ [28] where b is the characteristic monomer (Kuhn) size. The force on the segment, $f_{ch}^* \approx k_BT/b$, is high enough to align individual bonds in the direction of the relative motion in the $\hat{x}$-direction. Thus, vertical segment fluctuations in the $\hat{z}$-direction, which define the width of OZ, will be affected by the relative motion. As a result the OZ decreases with respect to its equilibrium value $\delta < \delta_0$ at $v > v_I^* \approx k_BT/b\zeta_0 g_0 \sim 1/g_0$ [28]. On the other hand, in a concentrated solution one may argue that the threshold velocity occurs at slower velocities and is given by $f_{ch}^* \approx \zeta_0 g v_{II}^* \approx k_BT/\delta_0$ that leads to $v_{II}^* \approx k_BT/b\zeta_0 g_{L/R}^{1+\nu}$ [26], where ν is the scaling exponent ($\nu = 1/2$ for an ideal chain and $\nu = 0.588$ for a swollen chain in 3D). In our simulations, hydrodynamic interactions are screened, therefore, we can take $\nu = 1/2$ and obtain $v_{II}^* \sim 1/g_0^{3/2}$. The ratio of two predictions for the threshold velocities obtained above is $v_I^*/v_{II}^* = g_0^{1/2}$. Unfortunately, in our simulations segment chain sizes inside the OZ are of the order of $g_{0L,0R} \sim 10$. Thus, we cannot capture a significant difference between the threshold-velocity predictions v_I^* and v_{II}^*. In principle, brush systems with larger $g_{0L,0R}$ values can be designed. However, for longer segment sizes, e.g. $g_{0L,0R} \approx 100$ chain entanglements will also come into play and introduce more complexities. Hence, throughout this work we will leave investigation of the threshold velocity v^* for a separate work [53], and refer v^* only to distinguish between the linear (any segment inside OZ is stretched less than its equilibrium size) and the non-linear force regimes (the segment end-to-end distance exceeds its equilibrium size).

As discussed above, at $v > v^*$ the segments inside the OZ are not Gaussian as they are stretched due to the relative motion of brushes, as illustrated by the snapshots given in Fig. 8. At the velocity range $v^* < v < v_{\max}$, where the maximum velocity that we considered here $v_{\max} \approx 1\ \sigma/\tau$, both δ_L and δ_R decrease in a similar way with increasing velocity as shown in Fig. 5. Thus, Eq. 6 is still valid to explain the difference in the frictional forces for velocities $v^* < v < v_{\max}$.

At around $v_{\max} \approx 1\ \sigma/\tau$, regardless of the brush topology, the width of the OZs goes to unity $\delta_{L,R} \to \sigma$ as shown Fig. 5. Hence, at $v \gtrsim v_{\max}$, according to Eq. 6, the ratio of friction forces for linear and ring brushes is

reduced to

$$\frac{f_L}{f_R} \approx \frac{\Omega_L}{\Omega_R}. \quad (7)$$

Indeed Fig. 7 shows that the ratio of binary-collision factors for ring and linear $\Omega_{L,R}$ is even higher at high velocities and reaches $\Omega_L/\Omega_R \approx 2$. The limit of $\delta_{L,R} \to \sigma$ for both ring and linear brushes at high velocities implies that there should be equal number of monomers inside the overlap volumes $\rho_m A\delta_{L,R}$. Additionally, from Fig. 6 we know that $g_R \approx 2g_L$. As $\delta_{L,R} \to \sigma$, this is only possible if stretched segments of ring brushes form double-stranded conformations inside the OZ as can be seen in the snapshot given for the non-linear regime in Fig. 8b. In the non-linear regime, a segment of ring brush with g_R monomers inside the OZ is highly stretched and adopts a double-stranded conformation. Due to double-stranding, each monomer of a segment in the ring brush has on average three neighbours from the same segment – two bonded and one non-bonded. Contrarily, a monomer inside the OZ in the linear brush has only two bonded neighbours in the non-linear force regime (Fig. 8d). The difference in conformation between linear and ring chains inside the OZ leads to smaller number of collisions between monomers from opposing layers in the latter case.

Another way of confirming that chain segments of ring brushes are double-stranded inside the OZ is to calculate the fraction of "participating" chains $\Psi_{L,R}$ (i.e. the fraction of these chains which occupy the OZ). Since linear chains has smaller number of monomers inside the OZ ($g_L < g_R$) larger number of chains should occupy the OZ to keep the monomer density ρ_m uniform throughout the simulation box. Calculated values of $\Psi_{L,R}$ according to previously described "participating" chain description are shown in Fig. 9 with ratios given in the insets. For slow velocities ($v < 10^{-1}\,\sigma/\tau$), which also correspond to the linear-force regime, Ψ_{0L} is slightly larger than Ψ_{0R} for all cases. On the other hand at high velocities ($v > v^*$) the difference between linear and ring brushes increases and is consistent with the conditions that $g_R > g_L$ and $\delta_{L,R} \to \sigma$. Note that in Fig. 9b, the increase in the ratio Ψ_L/Ψ_R is less pronounced. Possible reason is that our criterion for the participating chains can underestimate looping segments since we checked only whether the Nth monomer of the corresponding chain is within the OZ or not.

Finally, at ultra-high velocities $v \gg 1\ \sigma/\tau$, for which we cannot perform simulation since the thermostat cannot keep the system temperature uniform throughout the simulation box, one would expect that both $\delta_{L,R} \to \sigma$ and $\Omega_{L,R} \to 1$. Since the grafted chains are completely inclined and $g_{L,R} \to 1$, two opposing brushes can only interact via few monomers near the free edges of the grafted chains. This scenario indeed yields to a high-velocity linear regime and $f_L/f_R \to 1$.

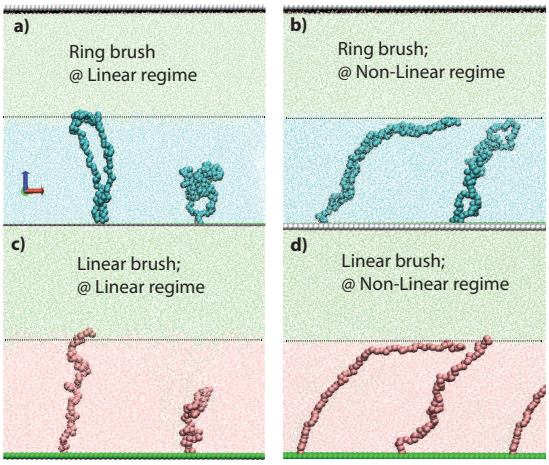

FIG. 8: Snapshots of the two arbitrarily-chosen chains from ring (a and b) and linear brush bilayers (c and d) simulations in the linear-force regimes (left column) and non-linear-force regimes (right columns). Polymerization degree of chains for linear brushes is $N = 60$, and for ring brushes is $N = 120$. Dotted lines indicate roughly the center of the overlap zones. Monomers of surrounding grafted chains are represented by dots. Top and bottom brushes were depicted with different colors.

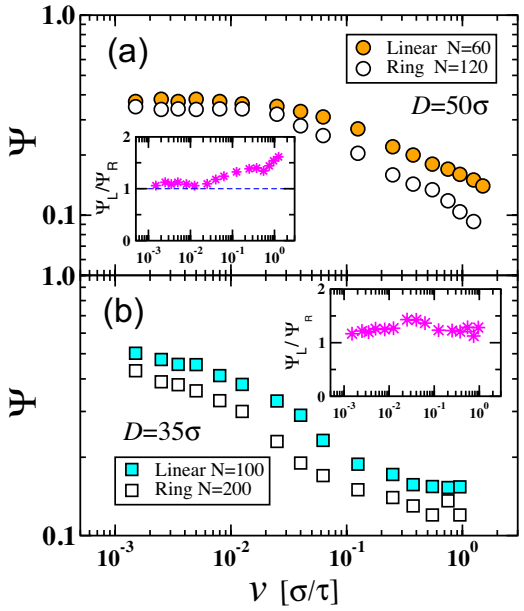

FIG. 9: The fraction of participating chains inside the overlap zone as a function of the plate velocity. Insets show the ratio of linear-brush data to ring-brush data. See text for details. The grafting densities are a) $\sigma_g^L = 0.25\sigma^{-2}$ and b) $\sigma_g^L = 0.11\sigma^{-2}$ with $\sigma_g^R = 0.5\sigma_g^L$.

CONCLUSION

In this work we demonstrated using scaling arguments and MD simulations that friction forces of linear chains are higher than those of ring brushes for a broad range of velocities spanning over three decades. For slow driving velocities (or shear rates), segments of a linear brush can penetrate through opposing brush deeper compared to segments of ring brushes. This is mainly due to the compactness of the segments in ring brushes. The compactness also decreases the number of collisions between two opposing ring brushes and results in lower frictional forces between two relatively moving brushes. For large driving velocities (shear rates), segments inside the overlap zone between brushes are highly stretched regardless of the topology of chains. In the ring brushes, stretched segments form double-stranded conformations which reduce the number of collisions with the monomers of the opposing brush.

We also observed that both friction forces and normal pressures in the linear chains are factor of two larger than those in ring brushes. This leads to equal kinetic friction coefficients $\mu = f/p$ for both systems. However, the effective viscosity $\eta_{\text{eff}} = f/v$ should be experimentally distinguishable for ring and linear chains.

A more interesting situation can arise when entangled brushes are considered. If chain segments can diffuse into the overlap volume with longer segments (around 100 monomers per chain for the bead-spring model), the segments of opposing brushes can entangle with each other. Since the bulk melts of ring chains exhibit no relaxation plateau in their stress-relaxation moduli [54, 55], their frictional responses should be much lower than those of entangled linear brushes. We will consider this scenario in a future publication.

We thank Edward J. Banigan and Ozan S. Sariyer for their careful readings of the manuscript. J.P. would like to thank G. Grest for pointing out several important numerical studies on the tribology of polymer brushes. This research was supported by the Polish Ministry of Science and Higher Education (Iuventus Plus: IP2012 005072). Computational time on the PL-Grid Infrastructure is gratefully acknowledged.

[1] P G De Gennes. Polymers at an interface; a simplified view. *Advances in Colloid and Interface Science*, 27(3):189–209, 1987.

[2] Jian Ping Gong. Friction and lubrication of hydrogels its richness and complexity. *Soft Matter*, 2(7):544, 2006.

[3] B N J Persson. *Sliding Friction: Physical Principles and Applications*. Springer Berlin Heidelberg, 2000.

[4] Neil Ayres. Polymer brushes: Applications in biomaterials and nanotechnology. *Polymer Chemistry*, 1(6):769, 2010.

[5] A Halperin. Polymer Brushes that Resist Adsorption of Model Proteins: Design Parameters. *Langmuir*, 15(7):2525–2533, March 1999.

[6] Feng Zhou and Wilhelm T S Huck. Surface grafted polymer brushes as ideal building blocks for ?smart? surfaces. *Physical Chemistry Chemical Physics*, 8(33):3815, 2006.

[7] Martien A Cohen Stuart, Wilhelm T S Huck, Jan Genzer, Marcus Müller, Christopher Ober, Manfred Stamm, Gleb B Sukhorukov, Igal Szleifer, Vladimir V Tsukruk, Marek Urban, Françoise Winnik, Stefan Zauscher, Igor Luzinov, and Sergiy Minko. Emerging applications of stimuli-responsive polymer materials. *Nature Materials*, 9(2):101–113, November 2019.

[8] Alexander Sidorenko, Sergiy Minko, Karin Schenk-Meuser, Heinz Duschner, and Manfred Stamm. Switching of Polymer Brushes. *Langmuir*, 15(24):8349–8355, November 1999.

[9] Philip Pincus. Colloid stabilization with grafted polyelectrolytes. *Macromolecules*, 24(10):2912–2919, 1991.

[10] EPK Currie, W Norde, and M A Cohen Stuart. Tethered polymer chains: surface chemistry and their impact on colloidal and surface properties. *Advances in Colloid and Interface Science*, 100:205–265, 2003.

[11] Uri Raviv, Suzanne Giasson, Nir Kampf, Jean-François Gohy, Robert Jérôme, and Jacob Klein. Lubrication by charged polymers. *Nature*, 425(6954):163–165, September 2003.

[12] M Urbakh, J Klafter, D Gourdon, and J Israelachvili. The nonlinear nature of friction. *Nature*, 430(6999):525–528, 2004.

[13] Jacob Klein, Eugenia Kumacheva, Diana Mahalu, Dvora Perahia, and Lewis J Fetters. Reduction of frictional forces between solid surfaces bearing polymer brushes. *Nature*, 370(6491):634–636, 1994.

[14] J. Klein. Repair or Replacement A Joint Perspective. *Science*, 323(5910):47–48, 2009.

[15] Meng Chen, Wuge H Briscoe, Steven P Armes, and Jacob Klein. Lubrication at physiological pressures by polyzwitterionic brushes. *Science*, 323(5922):1698–1701, March 2009.

[16] Bruno Zappone, Marina Ruths, George W Greene, Gregory D Jay, and Jacob N Israelachvili. Adsorption, Lubrication, and Wear of Lubricin on Model Surfaces: Polymer Brush-Like Behavior of a Glycoprotein. *Biophysical Journal*, 92(5):1693–1708, March 2007.

[17] Marcel Benz, Nianhuan Chen, and Jacob Israelachvili. Lubrication and wear properties of grafted polyelectrolytes, hyaluronan and hylan, measured in the surface forces apparatus. *Journal of Biomedical Materials Research*, 71A(1):6–15, 2004.

[18] N Maeda, N Chen, M Tirrell, and JN Israelachvili. Adhesion and friction mechanisms of polymer-on-polymer surfaces. *Science*, 297(5580):379, 2002.

[19] Debby P Chang, Nehal I Abu-Lail, Farshid Guilak, Gregory D Jay, and Stefan Zauscher. Conformational Mechanics, Adsorption, and Normal Force Interactions of Lubricin and Hyaluronic Acid on Model Surfaces . *Langmuir*, 24(4):1183–1193, February 2008.

[20] Xavier Banquy, Joanna Burdyńska, Dong Woog Lee, Krzysztof Matyjaszewski, and Jacob Israelachvili. Bioinspired Bottle-Brush Polymer Exhibits Low Friction and Amontons-like Behavior. *Journal of the American Chemical Society*, 136(17):6199–6202, April 2014.

[21] Debby P Chang, Nehal I Abu-Lail, Jeffrey M Coles, Farshid Guilak, Gregory D Jay, and Stefan Zauscher. Friction force microscopy of lubricin and hyaluronic acid between hydrophobic and hydrophilic surfaces. *Soft Matter*, 5(18):3438, 2009.

[22] Jeffrey M Coles, Debby P Chang, and Stefan Zauscher. Molecular mechanisms of aqueous boundary lubrication by mucinous glycoproteins. *Current Opinion in Colloid & Interface Science*, 15(6):406–416, December 2010.

[23] J Dorier and A Stasiak. Modelling of crowded polymers elucidate effects of double-strand breaks in topological domains of bacterial chromosomes. *Nucleic Acids Research*, 41(14):6808–6815, August 2013.

[24] Jonathan D Halverson, Won Bo Lee, Gary S Grest, Alexander Y Grosberg, and Kurt Kremer. Molecular dynamics simulation study of nonconcatenated ring polymers in a melt. I. Statics. *The Journal of Chemical Physics*, 134(20):204904, 2011.

[25] M E Cates and J M Deutsch. Conjectures on the statistics of ring polymers. *Journal de Physique*, 47(12):2121, 1986.

[26] A Galuschko, L Spirin, T Kreer, A Johner, C Pastorino, J Wittmer, and J Baschnagel. Frictional Forces between Strongly Compressed, Nonentangled Polymer Brushes: Molecular Dynamics Simulations and Scaling Theory. *Langmuir*, 26(9):6418–6429, May 2010.

[27] TA Witten, L Leibler, and PA Pincus. Stress relaxation in the lamellar copolymer mesophase. *Macromolecules*, 23(3):824–829, 1990.

[28] Alexander N Semenov. Rheology of Polymer Brushes: Rouse Model. *Langmuir*, 11(9):3560–3564, September 1995.

[29] J F Joanny. Lubrication by molten polymer brushes. *Langmuir*, 8(3):989–995, 1992.

[30] Jacob Klein. Shear, friction, and lubrication forces between polymer-bearing surfaces. *Annual review of materials science*, 26(1):581–612, 1996.

[31] Yangpeng Ou, Jeffrey Sokoloff, and Mark Stevens. Comparison of the kinetic friction of planar neutral and polyelectrolyte polymer brushes using molecular dynamics simulations. *Physical Review E*, 85(1), January 2012.

[32] L Spirin and T Kreer. Strongly Compressed Polyelectrolyte Brushes under Shear. *ACS Macro Letters*, 2(1):63–66, January 2013.

[33] Jan-Michael Y Carrillo, Daniel Russano, and Andrey V Dobrynin. Friction between Brush Layers of Charged and Neutral Bottle-Brush Macromolecules. Molecular Dynamics Simulations. *Langmuir*, 27(23):14599–14608, December 2011.

[34] Gary S Grest. Interfacial Sliding of Polymer Brushes: A Molecular Dynamics Simulation. *Phys. Rev. Lett.*, 76:4979, 1996.

[35] Gary S Grest. Normal and Shear Forces between Polymer Brushes. *Adv. Polym. Sci.*, 138:149, 1999.

[36] L Miao, H Guo, and MJ Zuckermann. Conformation of Polymer Brushes under shear: Chain Tilting and Stretching. *Macromolecules*, 29:2289, 1996.

[37] K. Binder, T. Kreer, and A. Milchev. Polymer brushes under flow and non-equilibrium conditions. *Soft Matter*, 7:2011, 2011.

[38] Benoît Liberelle and Suzanne Giasson. Friction and Normal Interaction Forces between Irreversibly Attached Weakly Charged Polymer Brushes . *Langmuir*, 24(4):1550–1559, February 2008.

[39] T. Kreer, M. H. Muser, K. Binder, and J. Klein. *Langmuir*, 17:7804, 2001.

[40] P.S. Doyle, E.S.G. Shagfeh, and A.P. Gast. *Macromolecules*, 31:5474, 1998.

[41] P. A. Schorr, T. C. B. Kwan, E. S. G. Shagfeh S. M. Kilbey, and M. Tirrell. *Macromolecules*, 36:389, 2003.

[42] F. Goujon, P. Malfreyt, and D. J. Tildesley. *Mol. Phys.*, 103:2675, 2005.

[43] F. Goujon, P. Malfreyt, and D. J. Tildesley. *Chem. Phys. Chem.*, 5:457, 2004.

[44] D. Irfachsyad, D. Tildesley, and P. Malfreyt. *Phys. Chem. Chem. Phys.*, 4:3008, 2002.

[45] D Reith, A Milchev, P Virnau, and K Binder. Anomalous structure and scaling of ring polymer brushes. *EPL (Europhysics Letters)*, 95(2):28003, June 2011.

[46] Fang Yin, Dmitry Bedrov, Grant D Smith, and S Michael Kilbey. A Langevin dynamics simulation study of the tribology of polymer loop brushes. *The Journal of Chemical Physics*, 127(8):084910, 2007.

[47] Kurt Kremer and Gary S Grest. Dynamics of entangled linear polymer melts: A molecular-dynamics simulation. *The Journal of Chemical Physics*, 92(8):5057, 1990.

[48] C Pastorino, T Kreer, M Müller, and K Binder. Comparison of dissipative particle dynamics and Langevin thermostats for out-of-equilibrium simulations of polymeric systems. *Physical Review E*, 76(2):026706, August 2007.

[49] Müller, M, MacDowell, and L Gonzalez. Interface and Surface Properties of Short Polymers in Solution: Monte Carlo Simulations and Self-Consistent Field Theory. *Macromolecules*, 33(10):3902–3923, May 2000.

[50] Steve Plimpton. Fast parallel algorithms for short-range molecular dynamics. *Journal of Computational Physics*, 117(1):1–19, 1995.

[51] W. Humphrey, A. Dalke, and K. Schulten. VMD program. *J. Molec. Graphics*, 14(1):33, 1996.

[52] Florent Goujon, Aziz Ghoufi, Patrice Malfreyt, and Dominic J Tildesley. Frictional forces in polyelectrolyte brushes: effects of sliding velocity, solvent quality and salt. *Soft Matter*, 8(17):4635–4644, 2012.

[53] A. Erbas, Zhulina E., and M. Rubinstein. Viscous friction of linear polymer brushes. in preparation.

[54] M Kapnistos, M Lang, D Vlassopoulos, W Pyckhout-Hintzen, D Richter, D Cho, T Chang, and M Rubinstein. Unexpected power-law stress relaxation of entangled ring polymers. *Nature Materials*, 7(12):997–1002, December 2008.

[55] Jonathan D Halverson, Won Bo Lee, Gary S Grest, Alexander Y Grosberg, and Kurt Kremer. Molecular dynamics simulation study of nonconcatenated ring polymers in a melt. II. Dynamics. *The Journal of Chemical Physics*, 134(20):204905, 2011.

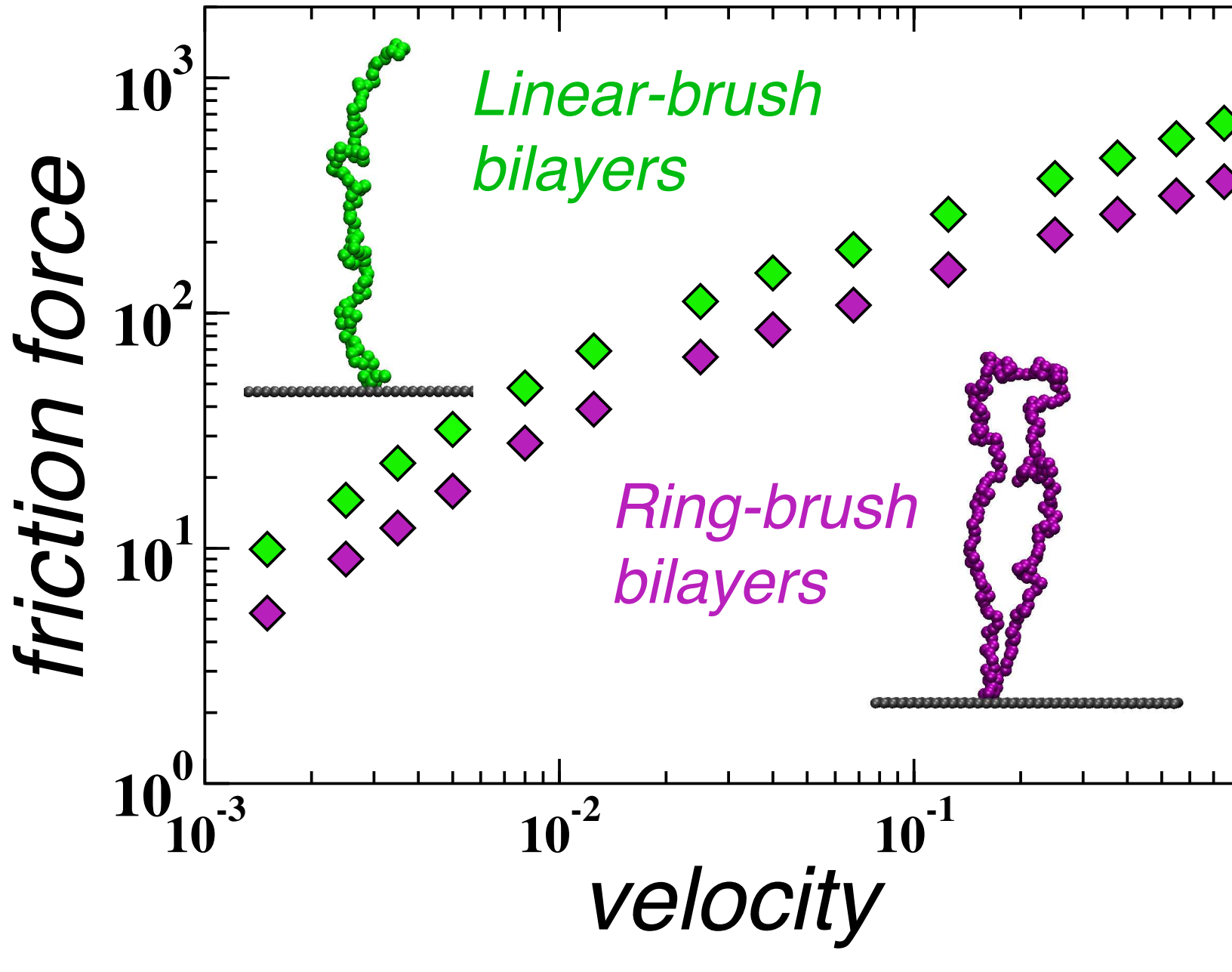
friction force
velocity
10^0
10^1
10^2
10^3
10^{-3}
10^{-2}
10^{-1}
Linear-brush bilayers
Ring-brush bilayers